Eur. Phys. J. B (2006)
DOI: 10.1140/epjb/e2006-00450-0

THE EUROPEAN PHYSICAL JOURNAL B

Acoustic signal associated with the bursting of a soap film which initially closes an overpressurized cavity

Experiment and theory

V. Vidal[1,a], J.-C. Géminard[2,b], T. Divoux[1], and F. Melo[1]

[1] Laboratorio de Física No Lineal and Center for Advanced Interdisciplinary Research in Materials (CIMAT), Departamento de Física, Universidad de Santiago de Chile (USACH), Avenida Ecuador 3493, Santiago, Chile

[2] Laboratoire de Physique, École Normale Supérieure de Lyon, 46 Allée d'Italie, 69364 Lyon Cedex 07, France

Received 3 May 2006 / Received in final form 10 November 2006
Published online 20 December 2006 –

Abstract. We report an experimental study of the sound produced by the bursting of a thin liquid film, which initially closes an overpressurized cylindrical cavity. There is a need for a deep understanding of the phenomenon, which can be very useful in numerous practical cases. For instance, in the nature, the volcanologists observe the bursting of large, elongated, gas-bubbles at the surface of lava lakes and record the associated sound emission. One can wonder which pieces of information they can get from such acoustic measurements. For a didactic purpose, we provide also the reader with all the theoretical background necessary for the understanding of the physical processes that govern the various characteristics of the acoustic signals: the cavity geometry governs the frequency; the viscous dissipation and the radiation are responsible for the damping; the acoustic energy informs about the characteristic time associated with the film-rupture more than about the energy initially loaded in the cavity.

PACS. 68.15.+e Liquid thin films – 43.20.Mv Waveguides, wave propagation in tubes and ducts – 43.20.Ks Standing waves, resonance, normal modes – 91.40.Yt Remote sensing of volcanoes

1 Introduction

The sound produced by the quick opening of an under- or overpressurized cavity is a common phenomenon. It can be encountered in many situations, from everyday life to large-scale natural systems.

One of the most well-known examples is certainly the characteristic 'pop' sound when opening a champagne bottle: the pressure inside the bottle, initially larger than the atmospheric pressure, drops down when the cork is released. Excited by the sudden change in pressure, the free volume close to the bottleneck resonates. In addition, the initial overpressure is due to a large amount of gas dissolved in the liquid, which, once the pressure has decreased, escapes the system as the famous champagne bubbles: by listening carefully to a glass full of champagne (or whatever 'bubbling' liquid), one can notice the soft popping sound generated by each bubble-bursting at the liquid surface. In this latter case, the resonators are the bubbles themselves.

To date, the studies of the sound emission have limited to the bursting of bubbles at the free surface of a newtonian fluid [1] in which, because of the rounded shape of the bubble reaching the free surface, the resonator consists of a liquid lens, the depth comparing with the bubble diameter [2]. By contrast, the body of a bubble rising in a non-newtonian fluid is likely to be strongly elongated along the vertical because of specific fluid rheological properties [3]. One can wonder about the characteristics of the sound emission in this latter case, which is relevant in various practical situations. For instance, the bursting of elongated bubbles can be observed in the kitchen, when cooking sauces [4]. Volcanoes are large-scale natural systems which exhibit very similar phenomena; a large amount of dissolved gas is released while lava rises up the magmatic

[a] *Permanent address*: Laboratoire de Physique, École Normale Supérieure de Lyon, 46 Allée d'Italie, 69364 Lyon Cedex 07, France.
[b] e-mail: jean-christophe.geminard@ens-lyon.fr

conduit [5]; bursting of large gas bubbles is sometimes observed at the surface of lava lakes or at vents. The characteristics of the acoustic signal beeing likely to provide useful pieces of information on the system geometry or dynamics, geophysicists have long been recording sound produced by volcanoes [6,7]. Because of the gas release, lava at the surface forms a foam having non-newtonian rheological properties. We can guess that one observes, at the surface of lava lakes, the bursting of bubbles that are elongated along the vertical.

One can then wonder what pieces of information can be extracted from acoustic measurements. We thus performed preliminary experiments in polymeric solutions and observed that, in some cases, the bursting of the thin film that initially closes the bubble at the free surface excites the elongated bubble body, which does not deform significantly during the sound emission and resonates like a tube [8]. We also observed a puzzling dependence of the acoustic energy on the bubble volume as well as, in the same experimental conditions, a large scatter of the acoustic energy. In order to account for the observations, it is fundamental to deeply understand the sound emitted as the consequence of the bursting of a well-controlled thin-film which initially closes an overpressurized cavity of well-defined geometry. Thus, we consider a resonating cavity consisting of a simple cylindrical-tube, closed at the bottom, which is excited by the bursting of a soap film at the top (Fig. 1). Previous studies of soap film bursting show that the typical film rupture is very fast [9], usually faster than all the physical processes inside and outside the cavity (acoustic resonance, radiation and sound wave propagation). Therefore, immediately after bursting, the characteristics of the sound waves, recorded inside and outside the resonating tube, depend generally on the tube geometry only. With this very simple experiment, we want to analyze the different physical mechanisms responsible for the temporal and spectral characteristics of the signal. We pay special attention in describing carefully the experimental procedures and propose in appendices all the theoretical tools and references necessary for the understanding of the phenomenon. We intend thus to provide the reader with useful and didactic material which, we hope, depending on his own interest, will help him in the interpretation of more complex systems, from the crackling of the champagne bubbles to the bursting of giant elongated bubbles on volcanoes.

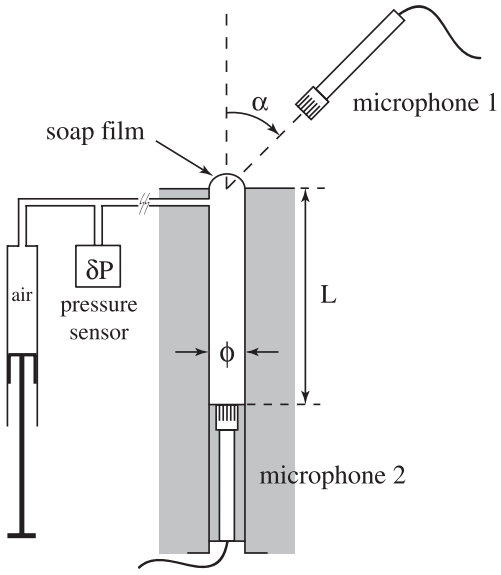

Fig. 1. Sketch of the experimental setup. The experimental setup consists of a tube (inner diameter ϕ) drilled in a plexiglass block. The length L of the cavity is tuned by changing the position of the microphone 2 (or rod) at bottom. The pressure difference δP across the film is controlled by means of a syringe pump and a pressure sensor. After the film bursting, the sound emitted outside the cavity is recorded with the help of the microphone 1 whereas the pressure at the bottom, which results from the standing waves inside the cavity, is monitored by using the microphone 2.

2 Experimental setup and procedure

The experimental setup consists of a vertical tube (diameter $\phi = 6, 8$ or 10 mm) drilled in a Plexiglass block (Fig. 1). The head of a first microphone (microphone ATM33a, Audio-Technica + preamplifier Eurorack UB802) is located $d = 5$ cm away from the upper-output plane and oriented at $\alpha \sim 45°$ from the system axis. At bottom, the system is either closed by means of a solid rod or by a second microphone (microphone 377A10 + preamplifier 426B03 + amplifier 482A16, PCB Piezotronics Inc.). Both the rod and the microphone at bottom are movable, in order to tune the cavity length L, from the output plane to the lower wall (from 2 to 23 cm).

At the top, an initially-flat soap-film is produced by stretching a droplet of a water-soap mixture (*Quix Limón*) with the help of a razor blade. Then, a capillary connected to the main vertical tube makes it possible to introduce a chosen volume of air from a syringe pump into the cavity limited by the lower wall and the film. A differential pressure transducer (PX277-01D5V, OMEGA Engineering Inc.) is used to measure the resulting pressure-difference, δP, across the soap film which then takes the shape of a part of sphere. In addition, the system can be imaged either from top or side with the help of a fast-camera (HiSIS 2002, KSV Instruments Ltd).

Subjected to gravity, the film thins (*drainage*, [10]) and, after a few tens of second, spontaneously bursts [11], which produces a characteristic sound. A digital oscilloscope (54602B, Hewlett Packard) is used to monitor and digitize the signals from the microphones (Fig. 2) and to transfer the raw data to a computer through the HPIB interface. Subsequent analysis is performed numerically (Matlab, The MathWorks, Inc. and Igor Pro, Wavemetrics, Inc.).

Thus, the experimental setup makes possible the analysis of the sound emission associated with the bursting of a curved soap film, which initially ends an almost cylindrical cavity of length L and diameter Φ filled with air

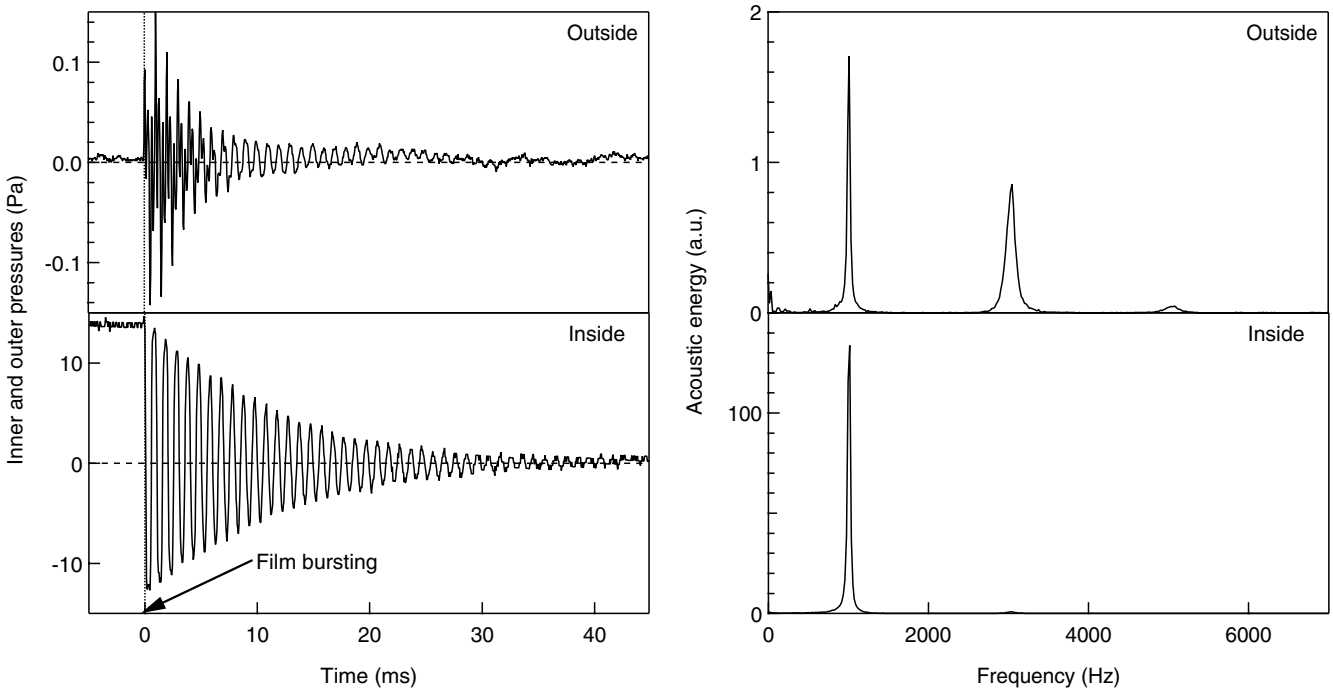

Fig. 2. Left: signals $P(t)$ from the microphones. Right: corresponding energy spectra. The typical signals from the two microphones exhibit, immediately after bursting of the film ($t > 0$), damped oscillations (left-hand-side). Note that the higher harmonics are damped faster in the signal from microphone 1. One can notice that their amplitude, relative to that of the fundamental, is larger outside (microphone 1) than inside (microphone 2) the cavity: even noticeable on the raw signals, this feature is clearly demonstrated by the energy spectra (*see* Appendix D for definition) displayed on the right-hand-side ($\delta P = 13.1$ Pa, $\Phi = 10$ mm, $L = 8$ cm, microphone 2 at the bottom, sampling rate 20 kHz).

at the overpressure δP above the pressure of the outside atmosphere. We shall report our experimental results and interpretations in the following Section 3 and draw conclusions in Section 4. The theoretical background necessary for the interpretation of our observations is presented in Appendices A to D.

3 Experimental results and interpretation

In the present section, we report our experimental observations, starting with the spectral analysis of the sound emitted after the bursting of the film (Sect. 3.1). We then discuss the temporal evolution of the amplitude (Sect. 3.2), focusing on the physical processes causing the temporal damping of the signal. In Section 3.3, we show that the analysis of the initial amplitude of the harmonics provides us with interesting pieces of information about the film rupture. Finally, the last Section 3.4 is dedicated to the energy balance.

3.1 Resonant frequencies ν_n

3.1.1 The fundamental frequency ν_0

From the experimental signals $P(t)$ provided by the microphone 1, we measure easily the fundamental frequency ν_0 of the acoustic wave in air, which corresponds to the lowest-frequency peak in the power spectrum (for instance, $\nu_0 \simeq 1$ kHz in Fig. 2). In order to analyze the effect of the cavity geometry, we shall report the results in terms of the associated wavelength λ_0, defined to be $\lambda_0 \equiv c/\nu_0$. Note that the velocity of sound in air, c, depends on the temperature T according to [12]:

$$c(T) = \sqrt{\frac{\gamma RT}{M}} \tag{1}$$

where $\gamma = 1.4$, $R = 8.14$ J K^{-1} mol^{-1}, and $M = 29$ g mol^{-1}. In our experimental conditions, the room temperature is about $T \simeq 298$ K and $c \simeq 346$ m s^{-1}.

Let us now tune the length L by changing the position of the microphone 2 (or rod) and determine the corresponding wavelength λ_0 of the fundamental. We observe that λ_0 depends linearly on L according to:

$$\lambda_0 = \xi(L + \delta L) \tag{2}$$

where $\xi = 4.00 \pm 0.05$ (Fig. 3) whatever the tube diameter Φ in our experimental range (6 to 10 mm). On the other hand, the length correction, δL, is observed to depend on the tube diameter Φ: for instance, we measure $\delta L = (4.2 \pm 0.1)$ mm in the case $\Phi = 10$ mm.

The tube, open at one end, constitutes a resonator which is excited by the pressure drop associated with the

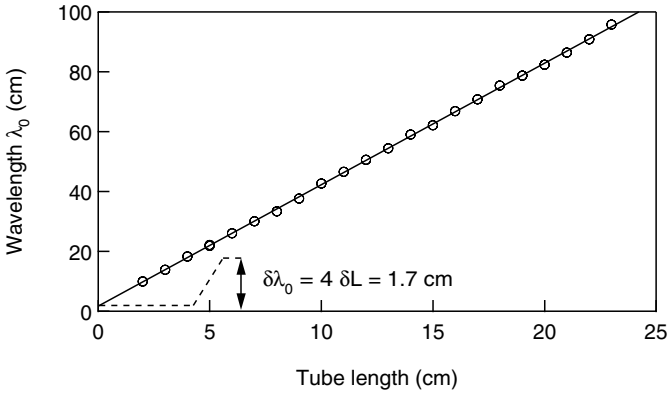

Fig. 3. Fundamental wavelength λ_0 vs. tube length L. The fundamental frequency ν_0 exhibited by the system after breaking of the soap film is associated with the wavelength λ_0, which is found to depend linearly on the tube length L according to equation (2) with $\delta L \simeq 0.42$ cm ($\Delta P = 10$ Pa, $\Phi = 10$ mm, rigid wall at the bottom, sampling rate 20 kHz).

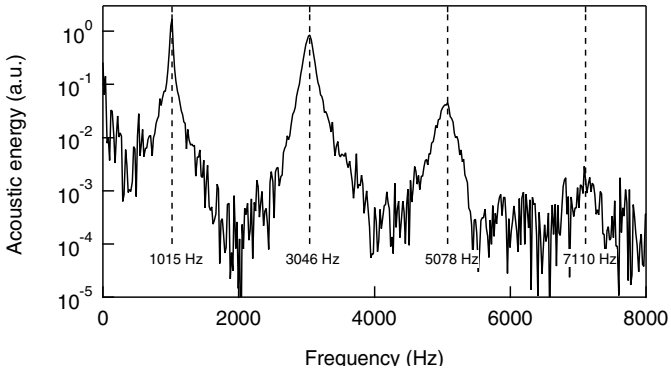

Fig. 4. Energy spectrum (microphone 1). We report, in log scale, the data from microphone 1 (Fig. 2). The vertical dashed lines clearly point out that the harmonics frequencies satisfy $\nu_n = (2n+1)\nu_0$ ($\delta P = 13.1$ Pa, $\Phi = 10$ mm, $L = 8$ cm, microphone 2 at the bottom, sampling rate 20 kHz).

sudden breaking of the soap film (Sect. A.5). What one can hear in air is the acoustic wave radiated outside the cavity (Appendix B) that selects the frequency (Appendix A). In a first approximation (Sect. A.1), we expect the pressure in the output plane to continuously equal the outside pressure (thus, a pressure node). At the bottom, we expect a velocity node and, accordingly, a pressure antinode. In this case, the cavity length equals one fourth of the fundamental wavelength and $\lambda_0 = 4L$. The experimental slope ξ is in fairly good agreement with this theoretical expectation (Fig. 3). However, the correction length δL is finite, as the pressure node does not exactly locate in the output plane. Indeed, because of the radiation of the acoustic wave in the output plane, one must consider the *effective* tube length $L' = L + \delta L$ where one expects $\delta L = 4\Phi/3\pi$ in the case of a flanged aperture [13,14] (Eq. (A.11)). One obtains a similar correction $\delta L = 0.3\ \Phi$, which is only slightly smaller than the latter, in the case of an unflanged aperture [13,15]. Experimentally, the correction length is found to be in fairly good agreement with the correction expected for a flanged aperture (we measure $\delta L \simeq 0.42$ cm for $\Phi = 10$ mm).

3.1.2 Higher-order harmonics ν_n ($n \neq 0$)

We point out that, in the theory (Sect. A.2.2), the correction δL is expected not to depend on the wavelength λ, so that the larger resonant frequencies ν_n are harmonics of the fundamental ν_0, $\nu_n = (2n+1)\nu_0$ associated with $\lambda_n = 4L'/(2n+1)$, where $L' = L + \delta L$. The prediction is well satisfied experimentally. Indeed, we observe clearly that the higher harmonics have frequencies that are odd multiples of the fundamental frequency: $3\nu_0$, $5\nu_0$, $7\nu_0, \ldots$ (Fig. 4).

3.1.3 Conclusion on the resonant frequencies

The characteristic frequencies of the sound wave emitted after the film bursting depend on the geometry of the resonant cavity only. Indeed, the signal recorded by the microphone 1 mainly contains the several harmonics of the fundamental ν_0, which is associated with the effective length $L' = L + \delta L$: L is the length of the cavity, from the bottom to the aperture plane, and δL a length correction, due to the radiation at the open end, which mainly depends on the tube diameter ϕ. In the next Section 3.2, we discuss the temporal envelope of the signal and, more specifically, how the amplitude of each of the harmonics vanishes.

3.2 Amplitude-damping characteristic-times τ_n

3.2.1 Qualitative observation

As can be seen on the signals $P(t)$, especially from microphone 1 (Fig. 2), the amplitude of harmonics associated with larger frequencies decreases faster. Indeed, the signal clearly contains several harmonics at short time (typically $t < 8$ ms) and only the fundamental afterwards (typically $t > 8$ ms). Measurements performed with a long enough cavity make it possible to determine with accuracy the characteristic time τ_n, over which the amplitude of the harmonic n vanishes, as a function of the corresponding frequency ν_n.

3.2.2 Analysis procedure

The analysis procedure is as follows: from the position of the peaks in the power spectrum (Fig. 4), we determine the fundamental resonant frequency ν_0. We then write the

signal from microphone 1 for $t > 0$:

$$P(t) = \sum_{n=0}^{\infty} A_n \sin(\omega_n t + \phi_n) \exp(-t/\tau_n) \qquad (3)$$

where $\omega_n = 2\pi(2n+1)\nu_0$. The interpolation of the experimental data with equation (3) provides us with the characteristic damping-time, τ_n, of each of the harmonics that exhibits a significant amplitude (thus generally up to $n = 2$). The agreement between equation (3) and the experimental data is excellent as shown, as an example, in Figure 5.

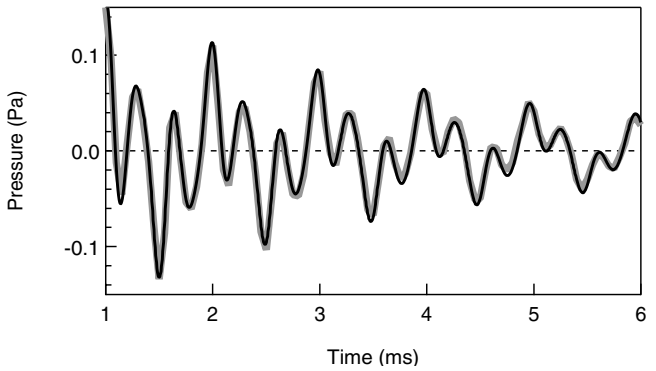

Fig. 5. Signal $P(t)$ from the microphone 1 vs. time t. Thick grey line: signal from the microphone. Thin black line: interpolation with equation (3). The experimental data are from Figure 2 ($\delta P = 13.1$ Pa, $\Phi = 10$ mm, $L = 8$ cm, microphone 2 at the bottom, sampling rate 20 kHz).

3.2.3 Experimental results

Each of the τ_n gives the experimental value of the characteristic damping time, τ_d, at the corresponding frequency $\nu = (2n+1)\nu_0$. Collecting the whole set of experimental measurements obtained for the various hamonics and different tube lengths L, we obtain the experimental τ_d as a function of the frequency ν. We checked that the experimental data reported in Figure 6 do not depend on the initial overpressure δP.

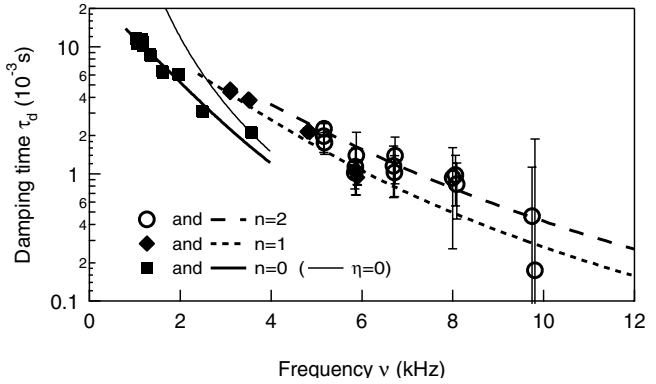

Fig. 6. Characteristic time τ_d vs. frequency ν. The data are obtained from the fundamental and its harmonics for various values of the cavity-length L, the diameter $\Phi = 8$ mm being kept constant (squares: fundamental $n = 0$; diamonds: first harmonic $n = 1$; open circles: second harmonic $n = 2$). The characteristic time τ_d decreases when the frequency ν increases as expected from equation (4) [the error bars are estimated from the interpolation of the experimental data with Eq. (3)]. The lines are obtained from equation (4) without any adjustable parameter (solid line: $n = 0$; long-dashed line: $n = 1$, short dashed line: $n = 2$). The thin continuous line points out the contribution of the radiation alone obtained from equation (4) with $\eta = 0$ ($\delta P = 18$ Pa, $\Phi = 8$ mm, rigid wall at the bottom).

3.2.4 Discussion

The radiation at the open end alone would lead to $\tau_d \propto \nu^{-3}$ (Sect. A.2.3), which is not observed experimentally, especially for small frequencies. We have evaluated other possible sources of dissipation [among them, the partial reflection at the closed end (Sect. A.3) and the thermal and viscous dissipation in the boundary layer at the vertical wall of the cavity (Sect. A.4)]. We estimated that, in the case of a rigid wall at bottom (rod), the damping of the acoustic wave due to the partial reflection at the closed end is negligible (this contribution must be taken into account when microphone 2 is placed at the bottom). Thus, taking into account only the radiation at the open end and the viscous and thermal dissipation in the boundary layer at the vertical wall of the cavity, we estimate the characteristic damping-time to be:

$$\frac{1}{\tau_d} = 2\frac{\sqrt{\pi\eta[1+(\gamma-1)P_r^{-\frac{1}{2}}]}}{\Phi}\nu^{1/2} + 2\pi^2\frac{\Phi^2}{c^2}\frac{\nu^3}{2n+1} \qquad (4)$$

where $\eta = 1.5 \times 10^{-5}$ m^2 s^{-1} denotes the kinematic viscosity of air, $P_r \simeq 0.7$, the Prandtl number, and $\gamma = 1.4$, the specific-heat ratio. Equation (4) gives, without any adjustable parameter, the characteristic damping-time which we find to be in rather good agreement with our experimental measurements (Fig. 6).

The damping of the standing wave inside the cavity is mainly governed by both the viscous and thermal dissipation at the wall, which dominates at small frequencies, and the radiation at the open end, which dominates at large frequencies. Whatever the dominant dissipation process, the harmonics having larger frequencies are damped faster. This is the reason why the sound, recorded outside, contains several harmonics right after the bursting of the film whereas only the fundamental is sensed later.

At this point, we know that the frequencies recorded by the microphone correspond to the resonant frequencies of the cavity and how the amplitude of the various harmonics vanishes when time increases. In the following Section 3.3, we discuss how the resonator is excited by the pressure drop associated with the film bursting and we show that a detailed analysis of the acoustic signal makes it possible to determine accurately the characteristic time of the resulting pressure drop in the aperture plane.

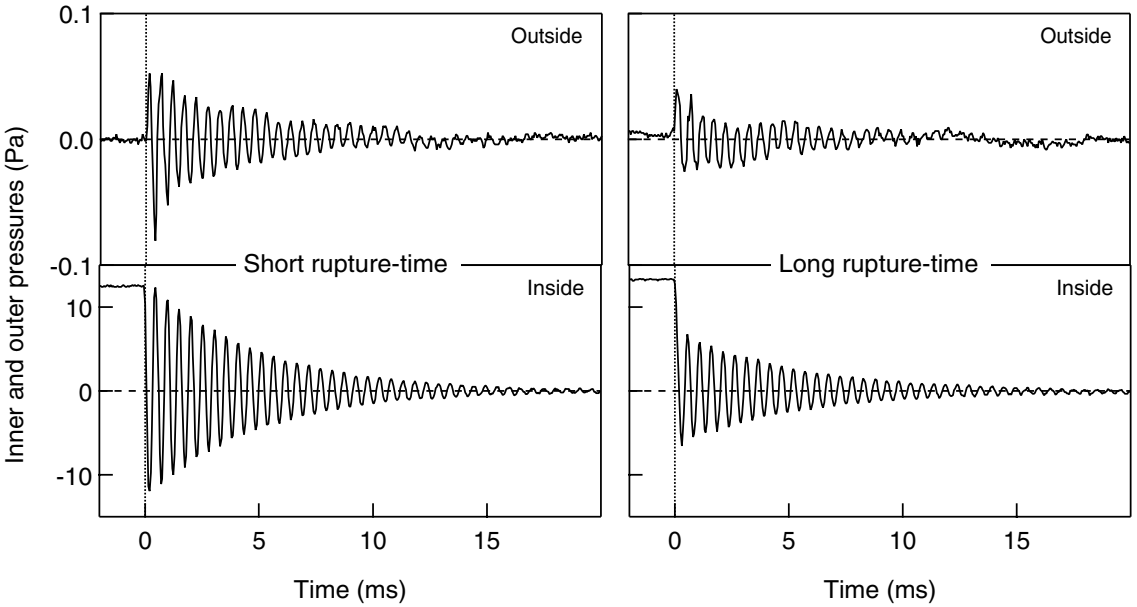

Fig. 7. Signals $P(t)$ from the microphones (top: microphone 1, bottom: microphone 2). Left: in the case of a short rupture-time, one observes that the overpressure at the closed end of the cavity goes from δP to $-\delta P$ immediately after bursting of the film. Right: if the rupture time is larger, the energy repartition among the acoustic modes is different, and the overpressure does not drop to $-\delta P$ immediately after bursting. Accordingly, the amplitude of the acoustic signal outside is smaller ($\delta P \sim 13$ Pa, $\Phi = 10$ mm, $L = 8$ cm, microphone 2 at the bottom, sampling rate 20 kHz).

3.3 Spectral analysis of the pressure drop associated with the film bursting

In this section, we obtain, from the detailed analysis of the coefficients A_n and ϕ_n which appear in equation (3), values of the Laplace transform of the pressure drop in the output plane and, consequently, the associated characteristic time, τ.

3.3.1 Qualitative observations

For identical initial conditions (given L, ϕ and δP), values of the initial amplitude of the acoustic signal can be very scattered. Even if the resonant frequencies are not affected, the acoustic signal varies significantly both in amplitude and shape, inside and outside the cavity (Fig. 7). This feature points out the fundamental role of the film breaking process in the excitation of the acoustic waves.

Using the fast camera, we observe the dynamics of the soap-film breaking, when not too fast, and we monitor the acoustic signal. We report in Figure 7, the acoustic signals obtained for two very different characteristic times of the film rupture. If the film rupture time is short, short enough for the soap film to disappear in the time between two images (1/4000 s), the amplitude of the signal inside the cavity initially drops down from $+\delta P$ to $-\delta P$ (Fig. 7, left). We note that this case corresponds to the rupture of a very thin film, which has reached the minimum accessible thickness [common black film (CBF, [10]) in our experimental conditions] before bursting. If the film rupture time is longer (in the same experimental conditions but, here, the drainage is not complete when the film breaks), the amplitude of the acoustic signal inside the cavity, right after bursting, does not drop down to $-\delta P$ anymore. Accordingly, the amplitude of the acoustic signal outside is smaller (Fig. 7, right).

In order to point out the variability of the amplitude of the acoustic signal from one experiment to another if one performs the experiment without controlling the thickness of the soap film when it breaks, we report measurements of the initial amplitude of the acoustic signal inside the cavity for two sets of experiments performed in the same experimental conditions (Fig. 8). One observes that the amplitude of the first oscillation is often much smaller than δP, especially for the shorter cavity.

In the next Section 3.3.2, we report experimental results obtained for the bursting of CBFs. In this latter case, the measurements are reproducible and we report a thorough analysis of the signal and draw conclusions.

3.3.2 Spectral analysis

The theoretical analysis (Sect. A.5.4) demonstrates that the amplitude and phase of the acoustic signal inside the cavity are related to the Laplace transform of the pressure drop $P(t)$ in the output plane which results from the film bursting. In what follows, we define $\hat{f}(s) \equiv \mathcal{L}[P(t)/\delta P - 1]$ where $\mathcal{L}$ denotes the Laplace transform. As the acoustic wave outside the cavity results from the radiation at the open end of the acoustic wave inside (Sect. B), we can estimate that the amplitude A_n and the phase ϕ_n of the

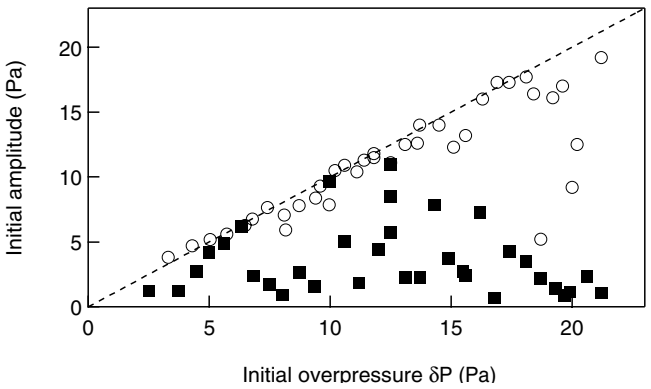

Fig. 8. Initial amplitude at the closed end vs. δP. We report the amplitude of the first oscillation of the pressure signal at the closed end of the cavity as a function of the overpressure δP for two different cavity lengths (full squares: $L = 2$ cm; open circles: $L = 8$ cm). Note that the scattering of the data, which is due to the variability of the bursting-film thickness, is largest for the shortest cavity length ($\Phi = 10$ mm, microphone 2 at the bottom).

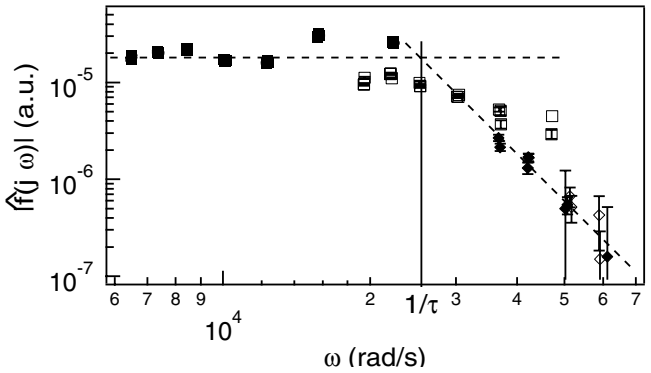

Fig. 9. Amplitude $|\hat{f}(jw)|$ as a function of ω. The experimental data are from the fundamental (full squares), the first (open squares), second (full diamonds) and third (open diamonds) harmonics. The amplitude is constant below and decreases like ω^{-5} above $\frac{1}{\tau}$ (vertical solid line). From the cut-off frequency, we obtain $\tau \simeq 40$ μs ($\delta P = 18$ Pa, $\Phi = 8$ mm).

signal from the microphone 1, located outside, satisfy:

$$A_n \propto \omega_n \left| \hat{f}(j\omega_n) \right| \tag{5}$$

$$\phi_n = \arg[\hat{f}(j\omega_n)] - \omega_n \left(t_0 + \frac{d}{c} \right) \tag{6}$$

where d denotes the distance between the microphone and the output plane [we introduce the time delay t_0 as, experimentally, the origin of time is taken when the signal exceeds a given threshold value and not when the film breaks. We thus expect t_0 to be of the order of magnitude of the signal period $2\pi/\omega_0$].

From the interpolation of the acoustic signal outside, we measure A_n and ϕ_n and, then, report the amplitude (Fig. 9) and the phase (Fig. 10) of $\hat{f}(jw)$ as a function of the frequency ω. At small frequency, both the amplitude and the phase are constant, whereas the amplitude decreases significantly (like ω^{-k} with $k \simeq 5$) above a typical

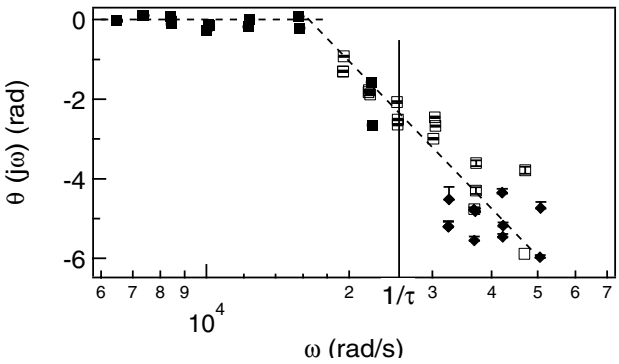

Fig. 10. Phase $\theta(j\omega) \equiv \arg[\hat{f}(j\omega_n)]$ as a function of ω. The experimental data set is the same as in Figure 9. In order to get a constant phase θ for $\omega < \frac{1}{\tau}$, we take $t_0 = 2.3 \times 10^{-4}$ s ($\delta P = 18$ Pa, $\Phi = 8$ mm).

value $1/\tau$ of the frequency ω. We observe a decrease in the phase $\theta \equiv \arg[\hat{f}(j\omega_n)]$ around the value $1/\tau$ but the scatter of the experimental data at large frequency avoids an accurate determination of the limit reached when $\omega \to \infty$. Nevertheless, the experimental results clearly exhibit a characteristic time τ associated with the pressure drop at the open end. We estimate $\tau \sim 40$ μs.

At this point, one could be tempted to recover the characteristic time τ in the signal recorded at the closed end of a long cavity. However, because of the dissipation at the side walls (Sect. A.4) which leads to a dispersive propagation (the harmonics have different velocity), the width of the initial pressure front, generated by the bursting of the soap film, increases during the propagation toward the closed end. As a consequence, the temporal behavior of the pressure from microphone 2 does not image what happened at the open end. As an experimental proof, we report results obtained for two different cavity-lengths (8 and 23 cm) and different viscosities of the soap film (Fig. 11).

The viscous soap films are obtained by mixing water, soap, sugar and glycerine. We observe with the fast camera that the characteristic rupture time is, at least, 2 to 3 times larger in this case. However, the first pressure drop measured at the closed end of the cavity looks very similar in the cases of the regular and viscous soap films, in the case of the longest cavity ($L = 23$ cm): the initial pressure drop associated with the film bursting is "hidden" by the widening of the pressure front during the propagation towards the closed end. Note also that the initial amplitude of the signal does not depend on the characteristic time τ of the pressure drop as, because of the choice of a long cavity, τ remains smaller than $1/\omega_0$. Making use of a different cavity length ($L = 8$ cm), we estimate from the data reported in Figure 11 the widening rate to be $\zeta \sim 15$ μs/cm.

Even if the pressure drop at the bottom does not exactly image the pressure drop at the open end, we can get an estimate of the rupture time τ in the case of a short cavity. For each signal, we determine the time τ_{drop} necessary for the pressure at the bottom to reach the first

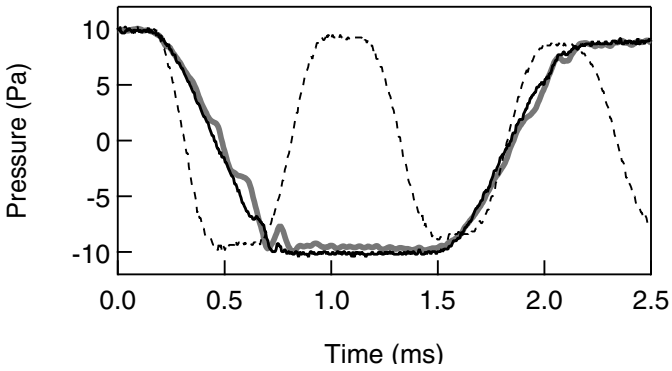

Fig. 11. Pressure $P(t)$ from microphone 2. Black solid line: regular soap film and $L = 23$ cm; thick grey line: viscous soap film and $L = 23$ cm; dashed line: viscous soap film and $L = 8$ cm. We report the first pressure drop (the origin of time is arbitrary). Even if the characteristic rupture time is 2 to 3 times larger for the viscous soap film (observation with the fast camera), one observes that the initial pressure drop at the closed end is almost the same for the regular and viscous soap films. By contrast, for the same characteristic rupture time, the initial pressure drop at the bottom drastically depends on the tube length L ($\delta P = 10$ Pa, $\Phi = 10$ mm).

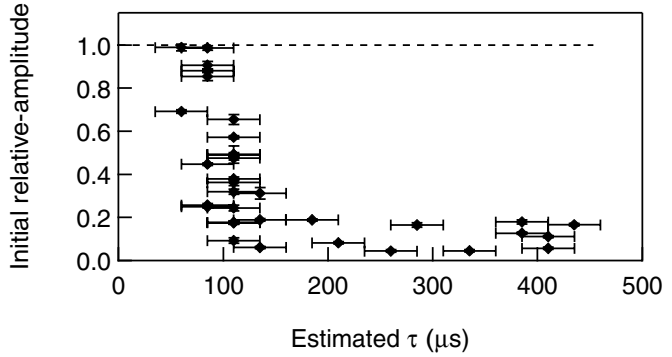

Fig. 12. Initial relative-pressure amplitude vs. estimated rupture time τ. The initial acoustic-signal amplitude is normalized to δP. The rupture time τ is estimated from the pressure drop at the bottom. In this experiment, $1/\omega_0 \sim 43$ μs ($L = 2$ cm, $\Phi = 10$ mm).

minimum. We estimate τ to be about $(\tau_{drop} - \zeta L)/2$. We report in Figure 12 the initial amplitude of the pressure signal, normalized to δP, as a function of the estimated τ. We observe, whatever the initial δP, a drastic decrease of the amplitude when the rupture time increases, which proves that the scattering of the data observed in Figure 8 is due to the variability of the rupture time.

Finally, we can compare the characteristic time τ measured in the experiment to an estimate of the typical time, τ_{typ}, expected for the opening of a film stretched over an aperture of radius $\Phi/2$. The opening of the film is driven by the surface tension and is limited either by the viscous dissipation [16] or by the inertia, this latter case being relevant in our experimental conditions. As a simple determination of the opening velocity appeared to be rather subtle [11], we detail here the model [17]. Let us now consider a pore of radius r which grows with the velocity v from the center of a frame (diameter $\phi/2$, Fig. 13). The liquid, initially located in the central disk of radius r, forms a rim of mass $m = \pi r^2 e\rho$, which grows with time (e stands for the film thickness and ρ for the density of the liquid). One could be tempted, at this point, to write the energy conservation by simply balancing the gain of surface free energy $2\Gamma\pi r^2$ ($\Gamma \simeq 30 \pm 2$ mN/m stands for the surface free energy of the liquid-air interface, the surface energy of the film is twice larger) with the kinetic energy $1/2mv^2$. However, if one considers the problem in the frame of reference of the rim (Fig. 13, inset), one can see that kinetic energy is continuously injected in inner flows (these flows are likely to be damped by the viscous dissipation but it is not nessecary to solve the hydrodynamical problem inside to go farther). We can easily see that the amount of kinetic energy which is introduced per unit time in the rim writes $2\pi erv \times 1/2\rho v^2$ ($2\pi erv$ corresponds to the volume of liquid, having the kinetic energy $1/2\rho v^2$ per unit volume, which enters the rim per unit time). As a consequence, the energy balance must be written:

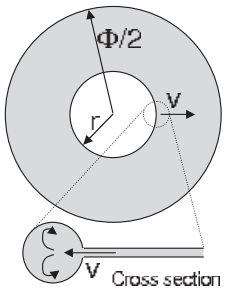

Fig. 13. Sketch of the opening pore.

$$2\Gamma \times 2\pi rv = \frac{d}{dt}\left(\frac{1}{2}mv^2\right) + 2\pi erv \times \frac{1}{2}\rho v^2. \qquad (7)$$

Taking into account the dependence of m on r, we obtain the constant velocity of the rim $v = \sqrt{2\Gamma/\rho e}$. Note that one half of the energy is dissipated and that an estimate of the velocity obtained without introducing the dissipation would be wrong by a factor $\sqrt{2}$ [11]. Assuming that τ_{typ} corresponds to the time the torus needs to reach the edge of the aperture, we get $\tau_{typ} = \frac{\Phi}{2}\sqrt{\rho e/2\Gamma}$. We can make use of $\tau_{typ} = \tau = 40$ μs to determine an estimate of the unknown film thickness. We get $e = 5.7$ nm, which is small but of the order of magnitude of the CBF thickness reported in the literature. We do not expect a quantitative agreement between τ_{typ} and τ as, first, there is no experimental proof that the bursting of the soap film corresponds to the opening of a pore at the center; second, as the relation between the dynamics of the pore opening and the associated pressure drop can be rather complex; and, finally, because the initial curvature of the soap film is not taken into account. Nevertheless, we note that τ_{typ} and τ are, at least, of the same order of magnitude, which is an indication that the acoustic measurements do provide a realistic estimate of the characteristic time associated with the pressure drop at the open end.

3.4 Energy transferred to the acoustic wave

The sudden breaking of the soap film produces a pressure drop inside the cavity. The total potential energy E_p released can be evaluated by considering the adiabatic expansion of the volume $V = \pi(\Phi/2)^2 L$ of gas when the inner pressure drops down by δP. One obtains $E_p = \frac{1}{2}\frac{V\delta P^2}{\rho c^2}$.

In the present section, we report how the energy E_p is transferred to the acoustic signal after the bursting of the soap film. Before reporting our experimental results, we discuss in Section 3.4.1 what the microphone 1 senses. The behavior of the total energy is analyzed in Section 3.4.2.

3.4.1 Preliminary remarks

The microphone 1 senses the acoustic signal $P(t)$ at a given point outside the cavity. As the acoustic wave outside the cavity is produced by a source of finite spatial extension (the surface area of the open end), the acoustic intensity $\mathcal{I}$ is likely to depend on the position of the microphone (distance and orientation) in a rather complex way.

Experimentally, the microphone is located at a finite distance $d = 5$ cm from the open end. One could worry the distance between the open end and the microphone to alter the amplitude of the various harmonics relative to each other. However, in our experimental conditions, the wavelength associated with the resonant frequencies is large compared to the cavity diameter and, as shown in Section B.1, the *far field* approximation applies. Thus, the amplitude associated with each of the modes decreases like $1/d$ where d is the distance to the open end, independent of the frequency. Moving the microphone toward or outward the tube end only rescales the power spectrum (as $1/d^2$) and does not modify the shape of the envelope.

On the other hand, the microphone is oriented at about 45 degrees from the cavity axis and we could also worry the spatial structure of the acoustic wave to alter the measurements. We show in Section B.2, that the angular dependence of the acoustic wave outside the cavity leads to a slight dependence of the acoustic intensity on the frequency for a given orientation of the microphone [Eq. (B.5)]. However, the correction is less than 10% in all our experimental conditions ($\Phi < 10$ mm, $\nu < 10$ kHz). In addition, we estimate from the first zero of the form factor that the modes having frequencies higher than about 40 kHz will not be sensed by the microphone.

The microphone is located at a finite distance from the tube aperture. One must, in principle, consider the spherical nature of the acoustic wave outside when estimating the acoustic energy from the pressure signal $P(t)$ provided by the microphone 1. However, we show in the appendix (Sect. A.5.7) that the total acoustic energy measured outside the cavity is given, to within better than 2.5% in all our experimental conditions, when neglecting the curvature of the wave front.

Finally, the typical lateral size of the experimental setup is less than d. It seems reasonable to assume that the spatial structure of the outside wave is a sphere and, thus, that the acoustic intensity is constant on the sphere of radius d. As a consequence, we estimate the total acoustic energy outside E_T^{out} to be simply given by

$$E_T^{out} \equiv \frac{4\pi d^2}{\rho c} \int_{t=0}^{\infty} P^2(t) dt, \tag{8}$$

where $P(t)$ is the pressure signal from the microphone 1. We expect the main source of error to be the integration over the sphere which leads to the prefactor 4π. Even if the potential error is there difficult to estimate, we can guess that E_T^{out} cannot overestimate the acoustic energy by more than 15% as we checked experimentally that the amplitude of the acoustic signal does not depend significantly on the angle α the microphone makes with the cavity axis, up to $\alpha \simeq 135°$.

3.4.2 Measurements and discussion of the energy balance

We already noticed that the soap film is likely to burst before having reached its minimum accessible thickness which leads to a scatter in the initial amplitude of the acoustic signals. We measured the acoustic energy E_T^{out} for different initial δP and report the data obtained when the film has reached its minimum accessible thickness (CBF) before bursting. In this case, the energy is maximum and the measurements are reproducible (Fig. 14).

We observe that $E_T^{out} \propto \delta P^2$ for small δP in agreement with $E_p \propto \delta P^2$. However, we note a departure from the quadratic law for larger δP. This feature is qualitatively explained by a change in the geometry of the film. Indeed, the film is almost flat at small δP and its bursting results in an almost-planar pressure-front propagating toward the cavity. In this case, the geometry of the front matches that of the planar modes inside the cavity and the energy transfer is efficient. By contrast, at large δP, the film bends significantly and its bursting results in a curved pressure-front propagating toward the cavity. The geometry of the front does not match that of the planar modes inside the cavity anymore and the efficiency of the energy transfer drops down.

More precisely, in the appendix A.5.7, we determine the input transmission coefficient for the energy:

$$T_i = \left| 1 - \left(\frac{x}{6j + x} \right) \left(\frac{1 - \cos\theta_0}{1 - e^{jx \tan\frac{\theta_0}{2}}} \right) \right|^2 \tag{9}$$

where θ_0 is defined by $\delta P = (8\Gamma/\Phi)\sin\theta_0$ and $x = \Phi/\lambda$. The dependence of T_i on δP accounts for the non-trivial behavior of E_T^{out}. Indeed, from the dynamics of the pressure drop at the open end and from E_p, the total energy transferred to the resonant modes inside the cavity, E_T^{in}, can be obtained by taking into account the transmission of each of the harmonics. In addition, we expect $E_T^{out} \propto E_T^{in}$, provided that only δP is varied. We observe that the dependence of E_T^{out} on δP, predicted from T_i, compares nicely with the experimental observations (lines

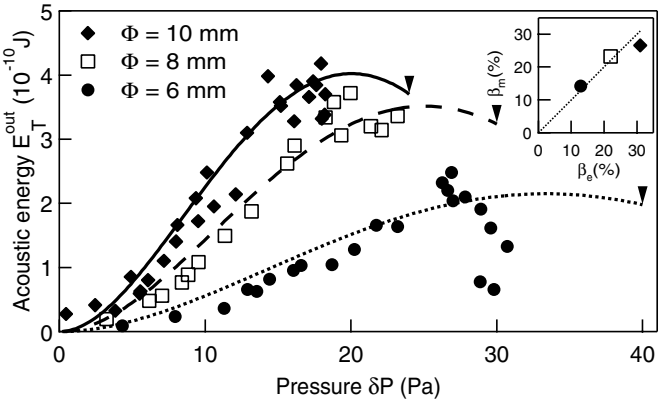

Fig. 14. Total acoustic energy outside E_T^{out} vs. initial overpressure δP. Whatever the cavity diameter Φ, the acoustic energy scales like δP^2 for small δP whereas a departure from the quadratic law is observed for large δP. The bending of the film accounts nicely (lines) for the experimental observations ($L = 5.5$ cm). Black arrows indicate the maximum $\delta P = 8\Gamma/\Phi$ for each of the diameters. In inset is plotted the percentage of energy we would measure outside (from the fit of the experimental points in this figure), as a function of the percentage of the energy expected to be measured, when excluding the geometrical effects. Note the good agreement between theory and the experimental observations.

in Fig. 14). The agreement proves that the geometry of the film is responsible for non-trivial dependence of the acoustic energy on the initial overpressure.

To go farther, we deduce from the interpolation of the experimental data the fraction $\beta = (1/T_i)E_T^{out}/E_p$ of the total energy E_p, that would be transferred to the acoustic modes outside the cavity in absence of the geometrical effects due to the bending of the film. Measured values β_m are reported in Table 1.

We can compare β_m to another estimate of β obtained, in addition, by considering the viscous dissipation and radiation only. On the one hand, assuming that the bursting of the film results in an exponential decrease of the pressure in the output plane with the characteristic time τ, one can estimate the amount of energy initially transferred to the acoustic modes inside the cavity (Sect. A.5.3) in absence of geometrical effects:

$$E_T^{in} = \Big[1 - \frac{2\omega_0\tau}{\pi}\tanh\Big(\frac{\pi}{2\omega_0\tau}\Big)\Big]E_p \equiv \beta_\tau E_p. \qquad (10)$$

Note that the fraction β_τ depends on the rupture time τ, which explains the scatter of the experimental data obtained when the film thickness is not controlled. In the case of a common black film, we estimated $\tau \sim 40$ μs for $\Phi = 8$ mm, which leads to $\beta_\tau \simeq 0.75$. As we expect τ to depend linearly on Φ, we can also report estimates of β_τ for $\Phi = 6$ and 10 mm in Table 1.

On the other hand, the total acoustic energy recovered outside, E_T^{out}, corresponds to the part of the energy E_T^{in} which is radiated and not dissipated at the walls. One can show that the fraction $\tau_n^{\mathcal{Z}}/(\tau_n^{\mathcal{Z}} + \tau_n^v)$ of the energy initially transferred to the mode n inside the cavity is dissipated

Table 1. Percentages β. Data in bold font are experimental values, whereas other data are estimates (see text).

Φ	6 mm	8 mm	10 mm
β_τ	81%	**75%**	68%
β_v	16%	**30%**	46%
β_e	13%	**22%**	31%
β_m	**14%**	**23%**	**26%**

at the cavity wall. We remind that τ_n^v and $\tau_n^{\mathcal{Z}}$ are the characteristic times associated with the dissipation at the wall and with the radiation at the open end, respectively. Defining $\beta_v = E_T^{out}/E_T^{in}$ and summing the contribution of all the harmonics, we obtain the expected value of β_v for $\Phi = 8$ mm. Taking into account the scaling behaviors of τ_n^v and $\tau_n^{\mathcal{Z}}$ on Φ, we get the estimates reported in Table 1 for $\Phi = 6$ and 10 mm.

Thus, from the dissipation at the wall and from the finite rupture time τ, we expect, in absence of the geometrical effects due to the bending of the film, $E_T^{out} \simeq \beta_e E_p$, with $\beta_e = \beta_\tau\beta_v$, which compares nicely to β_m (see inset Fig. 14). However, note that the agreement must be considered with caution, considering the uncertainty in measuring the characteristic time τ and in the surface of integration in equation (8).

As a conclusion of the energy study, we would like to underline again the strong influence of the film rupture time on the energy conversion. Hence, direct measurements of the acoustic energy do not provide any information on the energy initially loaded inside the cavity if the film rupture is unknown. Any attempt to do so would lead to false interpretations.

4 Conclusion and perspectives

We reported an experimental study of the acoustic signal associated with the bursting of a thin liquid film at the open end of a cylindrical cavity.

Let us first explain qualitatively why the signals from microphones 1 and 2 look so different. The radiation at the open end and the propagation inside the cavity are responsible for the drastic differences in the signals recorded at the bottom of the cavity and outside. Indeed, the transmission coefficient associated with the radiation is proportional to the frequency ν_n so that, at a given time t, the amplitude of the harmonic n, relative to that of the fundamental, is $(2n+1)$ times larger outside than inside the cavity. Moreover, the propagation along the cavity length makes the relative phase of two successive harmonics rotate by the angle π, so that, while in phase at the bottom, they have opposite phase in the output plane. The harmonics are thus clearly visible in the signal outside the cavity while they are hardly distinguishable in the signal recorded at the bottom. In addition, the harmonics are only observed at short times as they are damped faster mainly because of the radiation.

Our experimental findings can be summarized as follows:

- The acoustic signal exhibits a well defined fundamental frequency ν_0 which is mainly governed by the cavity length L. However, because of the radiation at the open end, the resonant length L', associated with the fundamental frequency ν_0, does not exactly equal the cavity length L but $L + \delta L$ where δL is a fraction of the tube diameter Φ.
- For long cavities, we observe a banded spectrum, with frequency peaks $\nu_n = (2n + 1)\nu_0$, where ν_0 is the fundamental frequency.
- Because of the radiation at the open end and of the thermal and viscous dissipation at the cavity walls, the acoustic signals we record inside and outside the cavity are damped in time. The associated characteristic times, we measure experimentally, are in fairly good agreement with the theoretical predictions without any adjustable parameter.
- The spectral content of the acoustic signals depends on how the cavity is opened. As a consequence, the careful analysis of the acoustic signal recorded outside the cavity makes it possible to determine accurately the characteristic time associated with the initial pressure drop at the open end of the cavity.
- The total amount of energy recovered in the acoustic signals depends drastically on the film curvature and on the dynamics of the film bursting.

We would like to emphasize once again the didactic goals of the work we reported herein. We were only aiming at the deep understanding of all the physical processes that govern the acoustic signals associated with the sudden opening of an under- or overpressurized cavity.

Focusing on one experimental situation, we can conclude that we can make use of the resonant cavity for performing the spectral analysis of the pressure drop associated with the film bursting. We are taught, for instance, that the bursting of a common black film, stretched over an 8 mm-in-diameter aperture, is associated with a characteristic time of about 40 μs.

Generalizing to other application fields, we can make use of our findings to better understand acoustic signals recorded in the nature. For instance, our study provides useful tools for the interpretation of the acoustic signals recorded on field by the volcanologists. First, the spectral content (frequencies) gives direct access to pieces of information about the geometry of the system: the resonant length relates to the bubble length whereas, from the surface, only the diameter of the bubble head or of the conduit can be observed. In the case of large bubbles bursting at the surface of a lava lake, the aspect ratio of the bubble depends on the rheological properties of the lava so that listening to the volcano makes it possible to access some rheological properties of the fluid. We point out that our experimental geometry is also relevant for interpreting the acoustic signal from the bursting of a giant elongated bubble at the top of a volcanic vent [7]. In this case the resonant length informs us about the conduit length and the damping characteristic-time about the processes that lead to the energy loss in the system, which gives constraints for modeling the resonant cavity [viscosity of the medium in which the acoustic wave propagates (gas or magma), material present at the closed end (either magma or solid rock from the reflection coefficient), etc.]. On the other hand, we point out some limitations of the acoustic methods: as they drastically depend on the film-rupture characteristic-time, which is neither a controlled nor a measured quantity in the field, the acoustic-signal amplitude and/or energy cannot be used to measure the total energy released during the bursting of a single bubble. Any attempts to do so would lead to misinterpretation of the field data.

The authors are very grateful to S. Vergniolle, M. Ripepe and D. Legrand for having provided us with exciting and useful pieces of information about the acoustics of volcanoes. We also highly thank S. Job, S. Douady, D. Constantin and B. Castaing for fruitful discussions. This work was supported by CONICYT under FONDAP Program No. 11980002 and FONDECYT Project No. 3040018. V. Vidal and J.-C. Géminard would like to thank the *Centre National de la Recherche Scientifique* (CNRS, France) and T. Divoux the *École Normale Supérieure* (ENS, Paris) for supporting the research of their members and students in foreign laboratories.

Appendix A: Theoretical background

A.1 The perfect resonant cavity

Let us denote $P(\mathbf{r}, t)$ the pressure field associated with the acoustic wave (P does not include the constant pressure P_a of the atmosphere). Denoting c the velocity of sound in air, we write the general equation governing an acoustic wave:

$$\Delta P - \frac{1}{c^2}\frac{\partial^2 P}{\partial t^2} = 0. \tag{A.1}$$

The particle velocity $\mathbf{v}$, associated with the pressure field $P(\mathbf{r}, t)$, obeys the relation:

$$\rho\frac{\partial \mathbf{v}}{\partial t} = -\nabla P. \tag{A.2}$$

Let us consider the cylindrical cavity [length L ($x \in [-L, 0]$), diameter Φ] initially ($t < 0$) filled with air at the pressure $P_a + \delta P$. We are aiming at the description of the evolution of the pressure field inside the cavity resulting from the opening of the cavity at one end ($x = 0$). We limit our study to the planar waves, $P(\mathbf{r}, t) = P(x, t)$, that can propagate in the cavity and ignore the higher-order, non planar, modes that could exist in the cavity but that are not relevant for our purpose [18].

Denoting $\hat{P}(x, s)$ the Laplace transform of $P(x, t)$, defined to be [19]

$$\hat{P}(x, s) = \int_0^\infty P(x, t)e^{-st}dt, \tag{A.3}$$

we obtain from the general equation (A.1),

$$\Delta\hat{P}(x,s)-\frac{s^2}{c^2}\hat{P}(x,s)=-\frac{s}{c^2}P(x,0)-\frac{1}{c^2}\frac{\partial P}{\partial t}(x,0). \quad (A.4)$$

Taking into account the initial condition $P(x,0)=\delta P$, $\forall x\in[-L,0[$, the general solution to equation (A.4) satisfies

$$\hat{P}(x,s)=A_+e^{\frac{sx}{c}}+A_-e^{-\frac{sx}{c}}+\frac{\delta P}{s} \quad (A.5)$$

where the constants A_+ and A_-, which are functions of s, are given by the boundary conditions at both ends.

Assuming that the reflection of the sound wave at the closed end (plane $x=-L$) occurs without any loss, the particle velocity along the x-axis, $v_x(-L,t)=0$ ($\forall t$). From the Laplace transform of equation (A.2),

$$s\hat{v}_x(x,s)-v_x(x,0)=-\frac{1}{\rho}\nabla\hat{P}(x,s), \quad (A.6)$$

and from the initial condition, $v_x(x,0)=0$ ($\forall x\in[-L,0[$), we get $\nabla\hat{P}(-L,s)=0$ ($\forall s$). As a consequence, $A_+=A_-$ and, thus,

$$\hat{P}(x,s)=A(s)\cosh\Big[\frac{s(x+L)}{c}\Big]+\frac{\delta P}{s} \quad (A.7)$$

where the amplitude A, which is a function of s, is given by the boundary condition at the open end.

In a first approximation, once the cavity is opened, the overpressure at $x=0$ instantaneously vanishes so that $P(0,t)=\delta P$ ($t<0$) and $P(0,t)=0$ ($t>0$) (we thus consider in this section that the output impedance at the open end is zero). As the consequence, the Laplace transform of the pressure at the open end $\hat{P}(0,s)=0$ and, from equation (A.7),

$$\hat{P}(x,s)=\frac{\delta P}{s}\left\{\frac{\cosh\big[\frac{s}{c}L\big]-\cosh\big[\frac{s}{c}(L+x)\big]}{\cosh\big[\frac{s}{c}L\big]}\right\}. \quad (A.8)$$

The solution for the pressure field $P(x,t)$ is obtained by calculating the inverse Laplace transform of $\hat{P}(x,s)$. The resonant frequencies are associated with the poles, $s_n=j(2n+1)\frac{\pi c}{2L}$ (n integer ranging from $-\infty$ to $+\infty$), which cancel the denominator $\cosh\big[\frac{s}{c}L\big]$ in equation (A.8). Thus, the *perfect* cavity (reflection without any loss at the closed end and zero output impedance) exhibits a series of resonant frequencies $\omega_n\equiv(2n+1)\frac{\pi c}{2L}$ which are associated with the wavelengths $\lambda_n\equiv\frac{c}{\nu_n}=\frac{4L}{2n+1}$.

Once the resonator has been excited due to the opening of the cavity at one end, one could expect to hear the resonant frequencies ω_n outside the cavity. However, as the frequencies ω_n correspond to perfectly resonant modes, by definition, the amplitudes of these modes do not decrease with time and, accordingly, no acoustic wave can exist outside the cavity. This conclusion, which contradicts the experimental observations, is the consequence of the specific boundary condition at the open end that we chose in this section: we considered that the pressure in the output plane is zero for $t>0$ (zero output impedance). As discussed in Appendix B, this assumption is not experimentally satisfied and the resonant modes can indeed escape the cavity, producing the acoustic wave that we can hear outside. In the next Section A.2, we will consider a more realistic boundary condition at the open end and analyze the consequences on the resonant modes inside the cavity.

A.2 Effect of the radiation at the open end

A.2.1 Introduction

Let us now assume that the output acoustic impedance, $\mathcal{Z}_r$, is finite (Appendix B) and that there exists acoustic waves inside and outside the cavity. Writing the continuity of the pressure and velocity fields in the output plane ($x=0$), we get:

$$\hat{P}(x,s)=\frac{\delta P}{s}\times\left\{1-\frac{\cosh\big[\frac{s}{c}(L+x)\big]}{\cosh\big[\frac{s}{c}L\big]+\frac{\mathcal{Z}_r(s)}{\rho c}\sinh\big[\frac{s}{c}L\big]}\right\} \quad (A.9)$$

which reduces to equation (A.8) in the limit $\mathcal{Z}_r(s)\to 0$.

A.2.2 Resonant frequencies

The resonant modes are again obtained by determining the poles of $\hat{P}(x,s)$. Using the expression (B.7) of the acoustic impedance $\mathcal{Z}_r$ determined in the case of a flanged aperture, we get the poles s_n which satisfy

$$\frac{1}{\tanh\big[\frac{s_n}{c}L\big]}=-\frac{\mathcal{Z}_r(s_n)}{\rho c}=-\frac{4\Phi}{3\pi c}s_n+\frac{\Phi^2}{8c^2}s_n^2. \quad (A.10)$$

Neglecting the second order term in equation (A.10), we obtain the corresponding wavelengths

$$\lambda_n=\frac{4}{2n+1}\Big[L+\frac{4}{3\pi}\Phi\Big] \quad (A.11)$$

where n is an integer ranging from 1 to ∞.

Thus, to the first order in Φ/L, the radiation at the open end leads to a slight increase in the wavelength λ_n and, accordingly, to a slight decrease in the frequency $\omega_n=2\pi c/\lambda_n$. In the case of a flanged aperture [20], the *effective* resonant length of the cavity is $L'=L+\frac{4}{3\pi}\Phi$ [Eq. (B.7)]. In the same way, we obtain $L'=L+0.3\,\Phi$ for an unflanged aperture [Eq. (B.8)].

A.2.3 Damping of the resonant modes

Taking into account the second order term in equation (A.10) and defining $\tau_n^{\mathcal{Z}}$ by $s_n\equiv j\omega_n-1/\tau_n^{\mathcal{Z}}$, we get

$$\tau_n^{\mathcal{Z}}=\frac{8cL}{\Phi^2\omega_n^2}=4\pi\frac{c^2}{\Phi^2}\frac{2n+1}{\omega_n^3}. \quad (A.12)$$

One can notice that $\tau_n^{\mathcal{Z}}$ independently depends on the cavity length L and on the harmonic in consideration (i.e. on n).

The radiation leads to the damping of the harmonic n, having the frequency ω_n, with a characteristic time $\tau_n^{\mathcal{Z}}$, which scales like ω_n^{-3}. Equation (A.12) holds true in the case of a flanged aperture. In the case of an unflanged aperture [13], the characteristic time associated with the radiation is expected to be twice longer, $2\tau_n^{\mathcal{Z}}$ [the real part of the output impedance is twice smaller, Eq. (B.8)].

A.2.4 Pressure field

By calculating the inverse Laplace transform of $\hat{P}(x,s)$ given in equation (A.9), we can write an approximate solution for the pressure field inside the cavity:

$$P(x,t) = \frac{4\delta P}{\pi} \times \sum_{n=0}^{\infty} \frac{(-1)^n}{2n+1} \cos\Big[\frac{\omega_n}{c}(L+x)\Big] \cos(\omega_n t) \exp\Big[-\frac{t}{\tau_n^{\mathcal{Z}}}\Big] \tag{A.13}$$

in which we neglect terms having amplitudes smaller than or of the order of $(\phi/L)^2\delta P$. Note that, from equation (A.13), $P(x,0) = \delta P,\ \forall x \in [-L, 0[$.

Equation (A.13) describes the inner pressure field in the case of an instantaneous opening of the cavity. Indeed, we consider the initial condition of constant pressure inside the cavity for $t < 0$ (the output impedance $\mathcal{Z}$ is thus infinite for $t < 0$) and assume that the output impedance is $\mathcal{Z}_r$ for $t > 0$. Thus, we assume that the output impedance drops down from the infinity to $\mathcal{Z}_r$ in an infinitely short time. We shall discuss the effect of the characteristic time of the cavity opening in Section A.5. However, at this point, we do prefer to analyze first two additional physical processes which lead to the damping of the resonant modes inside the cavity: the partial reflection at the closed end (Sect. A.3) and the viscous dissipation at the cavity walls (Sect. A.4).

A.3 Effect of partial reflection at the closed end

A.3.1 Pressure field

Up to now, we considered that the reflection at the closed end of the cavity occured without energy loss. However, because of finite acoustic impedance of the material the frame is made of or, especially, when using the microphone 2 at the bottom, part of the acoustic energy is lost in the plane $x = -L$.

Let us assume that a planar wave propagating toward the closed end is reflected partially as a planar wave propagating toward the open end with the reflection coefficient r_0. Assuming zero output impedance at the open end, we get:

$$\hat{P}(x,s) = \frac{\delta P}{s} \times \left\{1 - \frac{\cosh\big[\frac{s}{c}(L+x)\big] + \frac{1+r_0}{1-r_0}\sinh\big[\frac{s}{c}(L+x)\big]}{1\cosh\big[\frac{s}{c}L\big] + \frac{1+r_0}{1-r_0}\sinh\big[\frac{s}{c}L\big]}\right\}. \tag{A.14}$$

Note that equation (A.14) reduces to equation (A.8) in the limit $r_0 \to -1$.

A.3.2 Damping of the resonant modes

Defining $\tau_n^{r_0}$ such that $s_n \equiv j\omega_n - 1/\tau_n^{r_0}$ we get, from the real part of the poles, $\omega_n\tau_n^{r_0} = \frac{\pi}{2}\frac{1-r_0}{1+r_0}$ ($\lambda_n \gg \Phi$). Thus, the harmonics amplitude decreases exponentially with the characteristic time

$$\tau_n^{r_0} = \frac{1-r_0}{1+r_0}\frac{1}{4\nu_n}. \tag{A.15}$$

Note that, assuming that r_0 is real, the reflection at the closed end does not affect the resonant frequencies.

A.4 Effect of dissipation at the cavity walls

The shear viscosity of air is small and the damping of the acoustic wave due to viscous dissipation can usually be neglected. Indeed, the characteristic damping length for an acoustic wave in air is of about 300 m. However, the planar waves propagating inside the cavity are not compatible with the condition of zero velocity along the x-axis at the side walls and dissipation occurs in the boundary layer, in which air is subjected to important shear.

A.4.1 Physical background

The dynamical equation including the kinematic viscosity η writes

$$\frac{\partial \mathbf{v}}{\partial t} = -\frac{1}{\rho}\nabla P + \eta\Delta\mathbf{v} \tag{A.16}$$

which reduces to equation (A.2) in the limit $\eta = 0$. In cylindrical coordinates, let us consider that the velocity along the x-axis ($r = 0$) oscillates at the frequency ω with the amplitude $\overline{v}_\infty$. Assuming that the thickness of the boundary layer, L_{bl}, is much smaller than the cavity diameter Φ, one can neglect the curvature of the walls and write the velocity along the x-axis

$$\overline{v}_x(r) = \overline{v}_\infty\left\{1 - \exp\left[-\frac{(1+j)(\frac{\Phi}{2} - r)}{L_{bl}}\right]\right\} \tag{A.17}$$

where $L_{bl} = \sqrt{2\eta/\omega}$ ($\eta = 1.5 \times 10^{-5}$ m^2 s^{-1} stands for the kinematic viscosity of air). From equation (A.17), one can estimate the viscous stress applied by the side walls to

the fluid and write the force balance in the cross section of the cavity:

$$\rho\frac{\partial v_x}{\partial t} = -\frac{\partial P}{\partial x} - \rho\beta v_x \tag{A.18}$$

where $\beta = 1/\Phi\sqrt{8\omega\eta}(1+j)$ and v_x stands for the mean particle velocity along the x-axis in the cross section of the cylindrical cavity (note that Eq. (A.18) holds true only in the limit $L_{bl} \ll \Phi$ and in the harmonic regime).

A.4.2 Modified wave equation and pressure field

We can rewrite, from the dynamical equation (A.18) and from the mass conservation,

$$\frac{\partial \rho}{\partial t} + \frac{\partial(\rho v_x)}{\partial x} = 0, \tag{A.19}$$

the wave equation

$$\frac{\partial^2 P}{\partial t^2} - c^2\frac{\partial^2 P}{\partial x^2} = -\beta\frac{\partial P}{\partial t} \tag{A.20}$$

which takes into account the viscous dissipation in the boundary layers at the side walls. Accordingly, the pressure field inside the cavity, assuming zero output impedance and reflection without loss at the closed end, can be written

$$\hat{P}(x,s) = \frac{\delta P}{s}\left\{\frac{\cosh\big[KL\big] - \cosh\big[K(L+x)\big]}{\cosh\big[KL\big]}\right\} \tag{A.21}$$

where $c^2K^2 \equiv s^2 + \beta s$. Note that, in the limit $\beta \to 0$, $K = s/c$ and equation (A.21) reduces to equation (A.8).

A.4.3 Damping of the resonant modes

Seeking for the damped oscillatory-modes, we write $s = j\omega - 1/\tau$ and determine the resonant frequencies ω_n and the corresponding viscous-damping characteristic-times τ_n^v cancelling the denominator in equation (A.21).

Thus, assuming that the reflection at the closed end occurs without energy loss and zero output impedance, we estimate that the dissipation within the boundary layer slightly affects the resonant frequencies and, in addition, leads to the damping of the mode n inside the cavity over the characteristic time

$$\tau_n^v \simeq \frac{\Phi}{\sqrt{2\omega_n\eta}}. \tag{A.22}$$

The shear in the boundary layer induces temperature gradients. The associated thermal losses at the walls are accounted for by replacing η in equation (A.22) by $\eta[1+(\gamma-1)P_r^{-\frac{1}{2}}]$ where $P_r \simeq 0.7$ stands for the Prandtl number and $\gamma = 1.4$, the specific-heat ratio [20].

A.5 Response of the resonant cavity to a pressure jump at the open end

A.5.1 Introduction

In this section, we discuss how the energy initially loaded in the cavity is transferred, immediately after bursting of the soap film, to the resonant modes. In order to understand the behavior of the system, before generalization, we determine the solution in the simple case of an exponential decay of the pressure at the open end with the characteristic time τ. We assume $P(0,t) = \delta P e^{-\frac{t}{\tau}}$ $(\forall t > 0)$.

The Laplace transform of the pressure at the open end is given by $\hat{P}(0,s) = \frac{\tau\delta P}{1+s\tau}$ so that, from equation (A.7),

$$\hat{P}(x,s) = \frac{\delta P}{s}\left\{1 - \frac{\cosh\big[\frac{s}{c}(L+x)\big]}{(1+s\tau)\cosh\big[\frac{s}{c}L\big]}\right\}. \tag{A.23}$$

A.5.2 Pressure field

The solution is obtained from the poles of equation (A.23), which are $s = -1/\tau$ and $s_k = j(2k+1)\frac{\pi c}{2L}$ (k integer ranging from $-\infty$ to $+\infty$). After some algebra, we get:

$$\frac{P(x,t)}{\delta P} = \frac{\cosh(\frac{L+x}{c\tau})}{\cosh(\frac{L}{c\tau})}\, e^{-\frac{t}{\tau}} + \sum_{n=0}^{\infty} a_n \cos\left[\frac{\omega_n}{c}(L+x)\right]\sin\Big[\omega_n t + \theta_n\Big] \tag{A.24}$$

where we define the frequency ω_n, amplitude a_n and phase ϕ_n of the mode n:

$$\omega_n \equiv (2n+1)\frac{\pi c}{2L}, \tag{A.25}$$

$$a_n \equiv \frac{4}{\pi}\frac{\omega_0}{\omega_n}\frac{(-1)^n}{\sqrt{1+(\omega_n\tau)^2}}, \tag{A.26}$$

$$\tan(\theta_n) \equiv \frac{1}{\omega_n\tau}\ , \quad \phi_n \in [0, \frac{\pi}{2}[. \tag{A.27}$$

In the limit $\tau \to 0$, we recover equation (A.13) excluding the radiation at the open end (i.e. $\tau_n^{\mathcal{Z}} \to \infty$).

The first term in equation (A.24) corresponds to an exponential decrease of the pressure, at each position x in the cavity, with the characteristic time τ. This contribution does not correspond to a resonant mode but to the mean gas flow which escapes the cavity. By constrast, the terms in the sum correspond to the resonant modes. The amplitude a_n decreases when n increases and depends on the characteristic time τ: if $\omega_n\tau \ll 1$, $a_n \propto \omega_n^{-1}$ and, if $\omega_n\tau \gg 1$, $a_n \propto (\omega_n^2\tau)^{-1}$. The change in regime occurs at the characteristic frequency $\omega_c = 1/\tau$.

A.5.3 Energy injected in the resonant modes

The total amount of acoustic energy inside the cavity once opened, E_T^{in}, corresponds to the contribution of the terms

in the sum in equation (A.24). We remind that the density of acoustic energy equals $\frac{1}{2}\rho(v^2 + \frac{P^2}{\rho^2 c^2})$. After simple algebra, taking into account the relation (A.26) and integrating over the inner volume V, we get

$$E_T^{in} = \frac{1}{2}\frac{V\delta P^2}{\rho c^2}\Big[1 - \frac{2\omega_0\tau}{\pi}\tanh\Big(\frac{\pi}{2\omega_0\tau}\Big)\Big]. \qquad \text{(A.28)}$$

In the limit $\tau \to 0$, $E_T^{in} = \frac{1}{2}\frac{V\delta P^2}{\rho c^2}$. Note that E_T^{in} corresponds to the work necessary for increasing adiabatically the pressure inside the cavity by δP ($\chi_a \rho c^2 = 1$, where χ_a is the adiabatic compressibility of air [13]). Thus, if the typical duration of the pressure drop τ is short compared to the period $2\pi/\omega_0$ associated with the fundamental frequency ω_0, the total amount of potential energy initially loaded in the cavity is transferred to the acoustic modes. To the contrary, when the typical opening time τ increases, the energy transferred to the acoustic modes decreases according to equation (A.28) in the case of an exponential decay of the pressure in the output plane.

A.5.4 Generalization

The result reported in Section A.5.2 can easily be generalized to any behavior $P(0,t)$ of the pressure at the open end if one considers only the resonant modes.

Let us first define the functions $g(x,t) \equiv P(x,t)/\delta P - 1$ and $f(t) \equiv g(0,t)$. From equation (A.7), we get

$$\hat{g}(x,s) = \hat{f}(s)\frac{\cosh[\frac{s}{c}(L+x)]}{\cosh[\frac{s}{c}L]}. \qquad \text{(A.29)}$$

One can determine the solution $g(x,t)$ by calculating the inverse Laplace transform of $\hat{g}(x,s)$. Aiming solely at the description of the resonant modes, we consider the poles of $1/\cosh[s/cL]$ and not the poles of $\hat{f}(s)$ that correspond to a non-resonant part of the pressure field. Limiting thus our study to the oscillatory part of the pressure field, we write

$$g(x,t) = \sum_{n=0}^{\infty} a_n \cos\Big[\frac{\omega_n}{c}(L+x)\Big]\sin(\omega_n t + \theta_n) \qquad \text{(A.30)}$$

together with

$$a_n = \frac{4\omega_0}{\pi}(-1)^n\Big|\hat{f}(j\omega_n)\Big| \qquad \text{(A.31)}$$

$$\theta_n = \arg[\hat{f}(j\omega_n)]. \qquad \text{(A.32)}$$

Note that equation (A.30) reduces to the sum in equation (A.24) for $f(t) = \exp(-\frac{t}{\tau}) - 1$.

The amplitude and phase of the various harmonics are governed by the pressure drop at the open end: measuring the amplitude and phase of several harmonics makes it possible, in principle, to determine the Laplace transform $\hat{P}(0,s)$ of the pressure drop at the open end and, then, the pressure in the ouput plane $P(0,t)$ as a function of time. Finally, note that, if we denote E_T^{in} any value of the initial energy in the acoustic modes inside the cavity at $t = 0$, we obtain that $\hat{f}(s)$ satifies the condition

$$\sum_{n=0}^{\infty}\Big|\hat{f}(j\omega_n)\Big|^2 = \frac{\pi^2\rho c^2}{4V\omega_0^2}\frac{1}{\delta P^2}E_T^{in}. \qquad \text{(A.33)}$$

A.5.5 Radiation and damping of the resonant modes

The radiation at the open end (Sect. A.2), the partial reflection at the closed end (Sect. A.3) and the viscous dissipation at the cavity walls (Sect. A.4) lead the damping of the resonant mode in time. The partial reflection at the closed end and the viscous dissipation are not affected by the opening of the cavity for $t \geq 0$. To the contrary, the bursting of the soap film affects the evolution of the pressure at the open end with time and, thus, governs the characteristic time τ (the output impedance drops down from the infinity to $\mathcal{Z}_r$ during the opening of the film). The phenomenon can hardly be described in the theory and, seeking for simplicity, we will assume that the output impedance is $\mathcal{Z}_r$ for $t \geq 0$ and that the opening of the film only governs the characteristic time τ. We expect such an approximation to be valid as long as τ is smaller than the time needed by the acoustic wave to go back and forth from the open end to the closed end. This is to say as long as $\tau < 2L/c$ or $\omega_0\tau < \pi$, which is generally the case in our experimental conditions.

In this framework, we suggest to write from equation (A.30), the pressure field associated with the acoustic modes inside the cavity

$$\frac{P(x,t)}{\delta P} = \sum_{n=0}^{\infty} a_n \cos\Big[\frac{\omega_n}{c}(L+x)\Big] \times \sin(\omega_n t + \theta_n)\exp\Big[-\frac{t}{\tau_n^d}\Big] \qquad \text{(A.34)}$$

where a_n and ϕ_n are given by equations (A.31) and (A.32). The frequencies ω_n are associated with the modified wavelengths λ_n which takes into account the effect of the radiation [Eq. (A.11), we neglect here the slight shift of the resonant frequency due to the viscous dissipation at the cavity walls]. The damping characteristic-time τ_n^d, which appears in equation (A.34), is given by

$$\frac{1}{\tau_n^d} = \frac{1}{\tau_n^{\mathcal{Z}}} + \frac{1}{\tau_n^{r_0}} + \frac{1}{\tau_n^v} \qquad \text{(A.35)}$$

where the various characteristic times τ_n are from Sections A.2 to A.4.

A.5.6 Acoustic wave outside the cavity

From the solution inside the cavity [Eq. (A.34)], we can calculate the particle velocity in the output plane and thus, from equation (B.1), the pressure field, $P^{out}(r,t)$, outside the cavity (Sect. B). We first assume that the microphone is located far from the output plane, at a

distance d large enough ($d \gg \Phi$) for the *far field* approximation to be valid (Sect. B.1). Second, we assume that the wavelength λ_n, associated with the harmonics we consider, is large compared to the cavity diameter Φ so that the pressure field outside has the spherical geometry (Sect. B.2). Finally, the damping of the mode n is supposed to be slow enough for considering that the amplitude is constant over one period (i.e. $\omega_n \tau_n^d \gg 1$). In this framework, equation (B.1) can be used (the imaginary parts of ω and k are small and can be neglected) and the integration over the output plane reduces to a multiplication by the surface area of the cross section. Calculating the velocity $\overline{v}_x$ from the solution inside the cavity, we get

$$\frac{P^{out}(r,t)}{\delta P} = \frac{\Phi^2}{4Lr} \times \sum_{n=0}^{\infty} \omega_n \left|\hat{f}(j\omega_n)\right| \sin\left[\omega_n\left(t-\frac{r}{c}\right)+\theta_n\right] \exp\left[-\frac{t}{\tau_n^d}\right]. \tag{A.36}$$

We remind that $\theta_n = \arg[\hat{f}(j\omega_n)]$.

Thus, listening to the sound outside the cavity makes it possible to determine the amplitude and phase of the Laplace transform of the pressure drop in the output plane and, then, the pressure drop itself. Finally, we point out that the conclusion holds true only for the harmonics which satisfy the condition $\omega_n \tau_n^d \gg 1$. Considering the radiation only ($\tau_n^d = \tau_n^{\mathcal{Z}}$), we can rewrite this latter condition $(2n+1) \ll 1/\pi(4L/\Phi)^2$. The equality leads to $n = 10$ for the shortest and widest cavity we use in the experiments whereas we only sense harmonics up to $n = 3$. We can thus consider that equation (A.36) gives a fairly good estimate of the pressure field outside the cavity in our experimental conditions.

A.5.7 Total energy in the acoustic wave outside the cavity

Assuming that the pressure and, thus, velocity fields outside the cavity are spherical, we can write the general expression of the total acoustic energy that crossed a sphere of radius r from $t = 0$ to ∞

$$\begin{aligned} E_T^{out} &= 4\pi r^2 \int_{t=0}^{\infty} \mathcal{I} dt \\ &= 4\pi r^2 \int_{t=0}^{\infty} P^{out}(r,t) v^{out}(r,t) dt \end{aligned} \tag{A.37}$$

where $\mathcal{I}$ stands for the acoustic intensity. By principle, this integral must be independant of r.

Consider then first that r is much larger than the wavelength of the fundamental (we point out here that this is not experimentally the case as the microphone 1 is not located far enough from the output plane). In this case, the acoustic wave is locally planar so that the acoustic intensity reduces to $\mathcal{I} = {P^{out}}^2/(\rho c)$. Calculating the integral in equation (A.37), one obtains the general expression of the total energy in the acoustic wave outside as a function of $\hat{f}(s)$

$$E_T^{out} = \frac{\pi \Phi^4}{16 L^2} \delta P^2 \sum_{n=0}^{\infty} \tau_n^d \omega_n^2 \left|\hat{f}(j\omega_n)\right|^2. \tag{A.38}$$

The result must be independant of the distance r and E_T^{out} is the total amount of acoustic energy that crosses any surface surrounding the cavity aperture.

Equation (A.38) applies whatever the physical origin of τ_n^d. If the radiation is the only source of damping, $\tau_n^d = \tau_n^{\mathcal{Z}}$ and equation (A.38) reduces to

$$E_T^{out} = \frac{\pi \Phi^2}{4L} c \delta P^2 \sum_{n=0}^{\infty} \left|\hat{f}(j\omega_n)\right|^2 = E_T^{in} \tag{A.39}$$

where the second equality is obtained by using the condition (A.33). Thus, if the acoustic waves are only radiated at the open end, without any source of dissipation, the total amount of energy in the acoustic wave outside the cavity E_T^{out} equals the total amount of acoustic energy E_T^{in} initially loaded inside the cavity at $t = 0$. We recover here the energy conservation.

At last, we already noticed that the microphone 1 is located at a distance d from the open end which is not large in comparison to the wavelength λ_0 of the fundamental. As the microphone only provides us with the local pressure and not with the particle velocity, let us define an estimate of the total acoustic energy by

$$E_T^{approx} \equiv \frac{4\pi d^2}{\rho c} \int_{t=0}^{\infty} \left[P^{out}(d,t)\right]^2 dt \tag{A.40}$$

from equation (A.37) and assuming that the acoustic impedance is that of a planar wave. One can show that $E_T^{approx} = E_T^{out}[1 + \mathcal{O}(\pi^2 \Phi^2/64Ld)]$. Thus, we estimate that E_T^{approx} differs from E_T^{out} by less than 2.5% in all our experimental conditions ($\Phi \leq 1$ cm, $L \geq 2$ cm and $d = 5$ cm).

Appendix B: Radiation at the open end

Let us consider a planar wave which propagates inside the cavity toward the open end. When crossing the output plane $x = 0$, the sound wave can invade the whole half-space $x > 0$. Thus, the planar wave is diffracted at the open end. The phenomenon has been widely studied [14], and we will summarize below the main results, obtained in the "piston" approximation, that we need for discussing our experimental findings.

Assuming the pressure field depends on time like $e^{j\omega t}$, we can decompose, at the open-end, the incident planar-wave into an infinite number of infinitesimal source elements of the form

$$d\overline{P}(\mathbf{r}) = j\omega\rho \frac{\overline{v}_x}{2\pi} \frac{e^{-jk|\mathbf{r}-\mathbf{r}'|}}{|\mathbf{r}-\mathbf{r}'|} dS \tag{B.1}$$

where $\overline{v}_x$ is the axial component of the velocity field associated with the planar wave inside the cavity, $\mathbf{r}'$ the position of the source element in the aperture plane and dS an infinitesimal surface element around the source. Integration of equation (B.1) over the whole surface of the aperture leads to the pressure field outside the cavity.

B.1 Near field — far field regions

Consider first a point located on the x-axis. We get by integration the pressure amplitude

$$|\overline{P}(\mathbf{r})|\Big|_{\substack{y=0\\z=0}} = 2\rho c\overline{v}_x\Big|\sin\Big\{\frac{1}{2}kx\Big[\sqrt{1+\Big(\frac{\Phi}{2x}\Big)^2}-1\Big]\Big\}\Big|. \tag{B.2}$$

Thus, along the x-axis, the amplitude of the pressure wave oscillates when the open end is approached from large values of x. Moving toward the cavity, one encounters the first local minimum in the pressure amplitude at x_0 which satisfies

$$\frac{4x_0}{\Phi} = \frac{\Phi}{\lambda} - \frac{\lambda}{\Phi}. \tag{B.3}$$

The distance x_0 is a convenient demarcation between the *near field* region, in which the behavior of the pressure field is complicated, and the *far field* region, in which the pressure amplitude decreases monotically along the x-axis. Note that $x_0 < 0$ for $\lambda > \phi$, which means that, in this case, there is no *near field* region. In our experimental conditions, the length L of the cavity is always much larger than the diameter ϕ. As a consequence there is no *near field* region, at least for the fundamental and several harmonics having low enough frequency.

B.2 Spatial structure of the radiated wave

Consider now a point located far away from the aperture ($|\mathbf{r}| \gg \Phi$). We get by integration, to the leading order in Φ/r,

$$|\overline{P}(\mathbf{r})|\Big|_{|\mathbf{r}|\gg\Phi} = j\frac{\rho c}{8}\overline{v}_x\frac{\Phi}{r}k\Phi\; e^{-jkr}\mathcal{H}(\theta) \tag{B.4}$$

where $r = |\mathbf{r}|$ and $\mathcal{H}(\theta)$ denotes the dependence of the pressure amplitude on the angle θ ($\cos\theta \equiv \mathbf{x}\cdot\mathbf{r}$) given by:

$$\mathcal{H}(\theta) = 2\frac{J_1(\frac{k\Phi}{2}\sin\theta)}{\frac{k\Phi}{2}\sin\theta}. \tag{B.5}$$

In equation (B.5), J_1 denotes the first-order Bessel function of the first kind [19]. Thus, even in the *far field* approximation, the pressure field outside the cavity strongly depends on the angle θ. However, in our experimental conditions $\lambda \gg \Phi$ and, as discussed in the text (Sect. 3.4.1), our measurements do not depend on the angular position of the microphone 1.

B.3 Output impedance

We can make use of the "piston" approximation for evaluating the acoustic impedance at $x = 0$ of the acoustic wave outside the tube. To do so, we can calculate the pressure field in the plane of the aperture by integration of equation (B.1). A second integration makes it possible to estimate in the case of a flanged pipe, as done by Rayleigh [14,21], the mean value $\langle\overline{P}\rangle$, in the aperture plane, of the pressure $\overline{P}$ associated with the acoustic wave

$$\langle\overline{P}\rangle = 2j\rho c\overline{v}_x\int_0^\infty \frac{\big[J_1(\xi k\frac{\Phi}{2})\big]^2}{\xi\sqrt{\xi^2-1}}d\xi. \tag{B.6}$$

In the limit $\lambda \gg \Phi$, we get the acoustic impedance associated with the radiation at the open end in the case of a flanged pipe

$$\frac{\overline{\mathcal{Z}}_r}{\rho c} = \frac{\langle\overline{P}\rangle}{\rho c\overline{v}_x} \simeq \frac{1}{8}(k\Phi)^2 + \frac{4}{3\pi}jk\Phi. \tag{B.7}$$

Similar calculations by Levine and Schwinger [15] in the case of an unflanged pipe lead to a similar, but numerically different, expression

$$\frac{\overline{\mathcal{Z}}_r}{\rho c} = \frac{\langle\overline{P}\rangle}{\rho c\overline{v}_x} \simeq \frac{1}{16}(k\Phi)^2 + 0.3\; jk\Phi. \tag{B.8}$$

Because of the radiation, the acoustic impedance at the open end is non-zero.

B.4 Transmission coefficient

From the continuity of the pressure and velocity fields in the aperture plane, we can estimate energy transmission coefficient at the open end [13]. One obtains

$$T = \frac{1}{2}\frac{k^2\Phi^2}{[1+\frac{1}{8}k^2\Phi^2]^2 + [\frac{4}{3\pi}k\Phi]^2}, \tag{B.9}$$

in the case of a flanged aperture. In the limit $k\Phi \ll 1$, the transmission coefficient reduces to $T \simeq 1/2k^2\Phi^2$ (the approximation is better than 10% up to $k\Phi = 0.5$). Note that T is an increasing function of the frequency as long as $\lambda > \Phi$.

Appendix C: Input impedance

C.1 Qualitative analysis

The rather complex behavior of the total energy E_T as a function of the overpressure δP can be understood by considering the geometrical structure of the initial configuration (film shape). Indeed, before bursting, the soap film is spherical-shaped (radius R) and the pressure difference is $\delta P = 4\Gamma/R$ where Γ denotes the surface free-energy

associated with the liquid-air interface (the surface free-energy of the soap film is 2Γ whereas the total curvature of the film is $2/R$).

Qualitatively, for small δP, the film is almost flat and its bursting results in a pressure drop along an interface which has the geometry of the planar standing-waves inside the cavity; as a consequence, the planar front associated with the pressure drop penetrates easily the cavity and the energy E_T is proportional to δP^2 as one would expect (limit $\delta P \to 0$ in Fig. 14). When δP is increased, the center of curvature of the soap film approaches the aperture plane. The spherical geometry of the front differs from that of the planar modes inside the cavity; as a consequence, the spherical modes associated with the pressure drop hardly enter the cavity and the total energy transferred to the cavity E_T decreases.

C.2 Input impedance

In order to account for the whole behavior of E_T as a function of δP, consider first the initial geometry sketched in Figure C.1. We will work in spherical coordinates centered in O, the center of the spherical film. The initial pressure distribution, which writes $\delta P(r) = \delta P$ for $r < R$ and $\delta P(r) = 0$ for $r > R$, can be written as a sum of spherical modes centered in O. In the sake of simplification, we further assume that the film bursting leads to an homogeneous change in the pressure or velocity along the surface of the film. One can thus first consider one pressure mode propagating toward the cavity,

$$\delta\hat{P}(r,s) = \delta\hat{P}^0(s)\frac{R}{r}\ e^{\frac{s}{c}(r-R)}, \tag{C.1}$$

and the corresponding velocity-mode:

$$\hat{v}(r,s) = -\frac{\delta\hat{P}^0(s)}{\rho c}\Big(1-\frac{c}{sr}\Big)\frac{R}{r}\ e^{\frac{s}{c}(r-R)}. \tag{C.2}$$

Note that $\hat{P}^0(s)$ denotes the Laplace transform of the pressure drop associated with the film bursting. From equations (C.1) and (C.2), we can calculate, in the plane of the open end, the mean pressure:

$$\left\langle\Delta\hat{P}\right\rangle(s) = 8\delta\hat{P}^0(s)\frac{Rc}{s\Phi^2}\Big[1-e^{-\frac{sR}{c}(1-\cos\theta_0)}\Big] \tag{C.3}$$

and velocity along the x-axis:

$$\langle\hat{v}\rangle(s) = -8\frac{\delta\hat{P}^0(s)}{\rho c}\frac{R}{s\Phi^2}\Big[\cos\theta_0 - e^{-\frac{s}{c}R(1-\cos\theta_0)}\Big]. \tag{C.4}$$

where $R\sin\theta_0 = \Phi/2$. We deduce from (C.3) and (C.4), the input impedance $\mathcal{Z}_i$, which is associated with the homogeneous variations of the pressure and velocity in the plane of the open end:

$$\frac{\mathcal{Z}_i(s)}{\rho c} = -\frac{1-e^{-\frac{s}{c}R(1-\cos\theta_0)}}{\cos\theta_0 - e^{-\frac{s}{c}R(1-\cos\theta_0)}}. \tag{C.5}$$

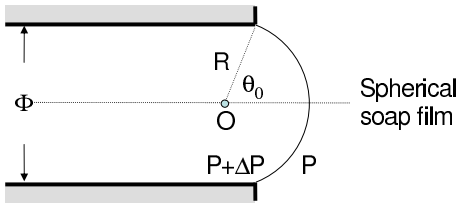

Fig. C.1. Sketch of the initial geometry.

C.3 Consequence — Transmission coefficient

Let us now consider that a fraction of the incident wave is transferred to a planar wave propagating toward the closed end (acoustic impedance $-\rho c$) while the remaining part is diffracted leading to a wave propagating away from the cavity [acoustic impedance in the plane of the open end, $\mathcal{Z}_r$ (Eq. B.7)]. Doing so, we implicitely assume that the characteristic time associated with the pressure drop is short compared with the time needed for the acoustic wave to go back and forth along the cavity length. Denoting $\hat{P}_c$ the amplitude of the wave transferred to the cavity and writing the continuity of the pressure- and velocity-fields in the plane of the open end, we get after some simple algebra:

$$\hat{P}_c(jw) = \hat{P}^0(jw)\left[1-\frac{x}{6j+x}\frac{1-\cos\theta_0}{1-e^{jx\tan\frac{\theta_0}{2}}}\right] \tag{C.6}$$

where $x \equiv \frac{\omega\Phi}{2\pi c} = \frac{\Phi}{\lambda}$. We remind that $\delta P = \frac{4\Gamma}{R} = \frac{8\Gamma}{\Phi}\sin\theta_0$ so that the transmission coefficient:

$$T_i \equiv \left|\frac{\hat{P}_c(jw)}{\hat{P}^0(jw)}\right|^2 = \left|1-\frac{x}{6j+x}\frac{1-\cos\theta_0}{1-e^{jx\tan\frac{\theta_0}{2}}}\right|^2 \tag{C.7}$$

is a function of the overpressure δP through $\theta_0(\delta P)$.

Appendix D: Energy spectrum

Let us now consider one damped harmonics which gives, directly from the microphone, the voltage $V(t)$ of the form:

$$V(t) = \overline{V}(\omega)\cos(\omega t)\ e^{-\frac{t}{\tau}} \tag{D.1}$$

Let us denote $t_k \equiv k/\nu_s$ the time samples with ν_s the sampling frequency. By definition, the fast Fourier transform of the signal writes:

$$FFT[V](n) \equiv \frac{1}{N^2}\sum_{k=0}^{N-1} V(t_k)\ e^{2\pi j\frac{kn}{N}}. \tag{D.2}$$

In what follows, we assume that the number of samples N is large (i.e. $N \gg \nu_s\tau$). We define the value of the energy spectrum $\Pi(\omega_n)$ at the frequency $\omega_n \equiv 2\pi\frac{n}{N}\nu_s$ by $\Pi(\omega_n) \equiv 2|FFT[V](n)|^2$. The spectrum Π, associated with the voltage given in equation (D.1), exhibits a maximum at:

$$\omega_n = \omega\left[\sqrt{1+\frac{4}{\omega^2\tau^2}} - \frac{1}{\omega^2\tau^2}\right]. \tag{D.3}$$

Thus, in the limit $\tau \to \infty$, $\omega_n = \omega$. In the presence of damping, in the limit $\omega\tau \gg 1$, the maximum is slightly shifted to a higher value ω_n such that $\frac{\delta\omega}{\omega} \equiv \frac{\omega_n - \omega}{\omega} \simeq \frac{1}{\omega^2\tau^2}$. The corresponding maximum value of the power spectrum is then given by:

$$\begin{aligned} \Pi(\omega_n) &= \overline{V}^2(\omega)\frac{\nu_s^2\tau^2}{4N^2}\Big[1+\sqrt{1+\frac{4}{\omega^2\tau^2}}\Big] \\ &\propto \frac{1}{2}\frac{\nu_s^2\tau^2}{N^2}\overline{V}^2(\omega) \quad (\omega\tau \gg 1). \end{aligned} \tag{D.4}$$

Note that, from its definition, Π depends on the acquisition time N/ν_s. In the limit $\tau \to \infty$, the acquisition time is smaller than τ and one must take $\tau = N/\nu_s$ in order to recover the expected value $\Pi = 1/2\overline{V}^2(\omega)$. In our experimental conditions, we choose the acquisition time to be large in comparison to τ and equation (D.4) applies.

References

1. D.E. Spiel, J. Geophys. Res. **97**, 11443 (1992)
2. H.M. Princen, *Surface and colloid science*, edited Matijevic, (Wiley-Interscience, NY, pp. 1–84 1969); Vol. 2, V. Bergeron, *Forces and structure in surfactant-laden thin-liquid films*, Thesis, University of California at Berkeley (1993)
3. A.A. Kulkarni, J.B. Joshi, Ind. Eng. Chem. Res. **44**, 5873 (2005)
4. M. Ichihara, T. Yanagisawa, Y. Yamagishi, H. Ichikawa, K. Kurita, *Japan Earth and Planetary Science Joint Meeting*, Abstract, (CD-ROM), A111-P004 (2005)
5. D. Dingwell, *Magma degassing and fragmentation: recent experimental advances*, in *From Magma to Tephra - Modelling physical processes of explosive volcanic eruptions*, Developments in Volcanology **4**, edited by A. Freundt, M. Rosi (Elsevier, 1998)
6. M. Ripepe, P. Poggi, T. Braun, E. Gordeev, Geophys. Res. Lett. **23**, 181 (1996)
7. S. Vergniolle, G. Brandeis, J. Geophys. Res. **101**, 20433 (1996); S. Vergniolle, G. Brandeis, J. Geophys. Res. **101**, 20449 (1996)
8. T. Divoux, *Listening to singing bubbles at the free surface of a non-newtonian fluid*, Stage de recherche de deuxième année du MIP, ENS, Paris (2004); T. Divoux, V. Vidal, J.-C. Géminard, F. Melo, *Optimal bubble size for noisy bubble bursting*, in preparation
9. N.Y. Liang, C.K. Chan, H.J. Choi, Phys. Rev. E **54**, 4, R3117 (1996)
10. K.J. Mysels, K. Shinoda, S. Frankel, *Soap films: studies of their thinning and a bibliography* (Pergamon, Oxford, UK, 1959)
11. S. Frankel, K.J. Mysels, J. Phys. Chem. **73**, 3028 (1969)
12. J. Backus, *The acoustical foundations of music*, 2nd edn. (W.W. Norton Co, Inc., New York, 1977)
13. L.E. Kinsler, A.R. Frey, A.B. Coppens, J.V. Sanders, *Fundamentals of acoustics*, 3rd edn. (J. Wiley & Sons, Inc., New-York, 1982)
14. J. Kemp, *Theoretical and experimental study of wave propagation in brass musical instruments*, Ph.D. thesis, University of Edinburgh (2002), and references therein
15. H. Levine, J. Schwinger, Phys. Rev. **73**, 383 (1948)
16. G. Debrégeas, P. Martin, F. Brochard-Wyart, Phys. Rev. Lett. **75**, 3886 (1990)
17. F.E.C. Culick, J. Appl. Phys. **31**, 1128 (1960)
18. A higher-order (non-planar) mode can only propagate if the associated frequency $\omega > \omega_c$, where $\omega_c \sim c/\Phi$ (i.e. the associated wavelength is of the order of or smaller than the cavity diameter) [14]. In our experimental condition the cavity length (and thus, the wavelength of the few first hamonics we listen to) is always much larger than the cavity diameter
19. G.B. Arfken, H.J Weber, *Mathematical method for physicists*, 4th edn. (Academic Press, 1995)
20. A. Pierce, *Acoustics - An introduction to its physical principles and applications* (ASA, New-York, 1989)
21. Lord Rayleigh in *Theory of sound* (Macmillan, 1940)